iScience

Article

Substantia nigra modulates breathing rate via locus coeruleus

Graphical abstract

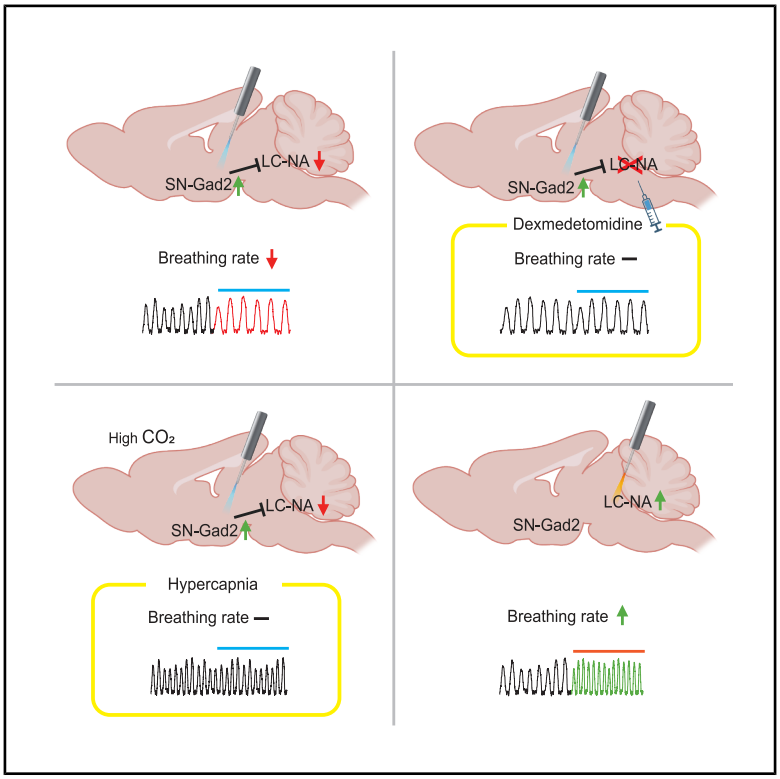

Highlights

- Gad2-expressing SN neurons modulate breathing rate
- Optogenetic activation of Gad2-expressing SN neurons reduces LC-NA neuron firing
- SN-modulated breathing depends on baseline LC-NA neuron activity and hypercapnia
- Direct stimulation of NA cells in LC increases breathing rate

Authors

Bon-Mi Gu, Jae Gon Kim, Aronee Hossain, Greg O. Cron, Jin Hyung Lee

Correspondence

ljinhy@stanford.edu

In brief

Neuroscience; Cellular neuroscience

Gu et al., 2025, iScience *28*, 112423
May 16, 2025
https://doi.org/10.1016/j.isci.2025.112423

CellPress

iScience

CellPress
OPEN ACCESS

Article

Substantia nigra modulates breathing rate via locus coeruleus

Bon-Mi Gu,[1,5] Jae Gon Kim,[1,5] Aronee Hossain,[1] Greg O. Cron,[1] and Jin Hyung Lee[1,2,3,4,6,*]
[1]Department of Neurology and Neurological Sciences, Stanford University, Stanford, CA 94305, USA
[2]Department of Bioengineering, Stanford University, Stanford, CA 94305, USA
[3]Department of Neurosurgery, Stanford University, Stanford, CA 94305, USA
[4]Department of Electrical Engineering, Stanford University, Stanford, CA 94305, USA
[5]These authors contributed equally
[6]Lead contact
*Correspondence: ljinhy@stanford.edu
https://doi.org/10.1016/j.isci.2025.112423

SUMMARY

Breathing is an automatic and rhythmic act primarily controlled by hindbrain neural circuits, including the pre-Bötzinger complex. While the basal ganglia are known to regulate a wide range of behaviors through downstream projections, their role in breathing control remains unclear. In this study, we demonstrate that outputs from the substantia nigra (SN) can modulate breathing rate in a cell-type specific manner. Specifically, optogenetic activation of glutamic acid decarboxylase 2 (Gad2)-expressing neurons in the SN, but not parvalbumin (Pvalb)-expressing neurons, decreased breathing rate in lightly anesthetized mice. Importantly, this effect was mediated through the inhibition of neural activity in the locus coeruleus (LC), suggesting a relationship between the decrease in breathing rate and the baseline firing rate of LC neurons. These findings provide evidence that the basal ganglia play an important role in the control of breathing rate through modulation of LC neural activity.

INTRODUCTION

The basal ganglia exerts control over many aspects of behavior, including decision-making, reward processing, behavioral inhibition, and movement.[1–7] The output nucleus of the basal ganglia, the substantia nigra pars reticulata (SNr), sends diverse projections to areas known for movement control such as the thalamus and superior colliculus.[8–10] The SNr also sends multiple outputs to various midbrain and brainstem targets,[11,12] but the role of these circuits remains unclear.

A few studies have hinted at a relationship between basal ganglia and respiration. Patients with Parkinson's disease, a basal ganglia disorder,[13] often have respiratory problems including sleep apnea.[14–16] Altered respiratory patterns in a 6-hydroxydopamine (6-OHDA) rodent model of Parkinson's disease were observed at rest and under hypercapnia conditions.[17,18] However, it is not clear if respiratory problems associated with Parkinson's stem from a centralized abnormality or peripheral dysfunction.[14] There are only limited reports on the direct relationship between basal ganglia and respiration controls.[19]

Breathing is primarily controlled by the respiratory neural network, including the pontine respiratory group and ventral respiratory column in the brain stem.[20] However, arousal, negative emotion, physical exercise, and chemical response can also modulate breathing.[21–23] Multiple upstream targets (e.g., amygdala) and neurotransmitters (serotonin, norepinephrine, etc.) are known to affect respiration.[22,24–27] In particular, the locus coeruleus (LC), which releases norepinephrine, plays a critical role in control of arousal levels[28,29] and respiratory changes.[27] It has been suggested that the LC acts as a chemosensitive vigilance center, detecting CO_2 or pH levels and triggering reflexive changes in breathing.[25,30,31]

In this study, we examined the influence of the substantia nigra (SN) on breathing rate and on LC cell activities. We specifically targeted glutamic acid decarboxylase 2 (Gad2)-and parvalbumin (Pvalb)-expressing GABAergic cells in the SN, including both the SNr and the adjacent substantia nigra pars compacta (SNc). Functional dissociations between Gad2-and Pvalb-expressing SN cells have been reported in sleep-wake states.[12] Optogenetically stimulated Gad2-expressing SN cells have been shown to induce sleep and decrease movement initiation, while Pvalb-expressing SN cells do not. Here, we hypothesized that specific SN cell types control breathing rate through the engagement of LC. Our goal was to investigate the potential role of basal ganglia in breathing rate control.

RESULTS

Optogenetic stimulation of Gad2-expressing SN cells reduces breathing rate

To investigate whether the SN modulates breathing rate and/or heart rate, we stimulated specific SN cell types in anesthetized Gad2-Cre or Pvalb-Cre mice (schematic in Figure 1A). Virus

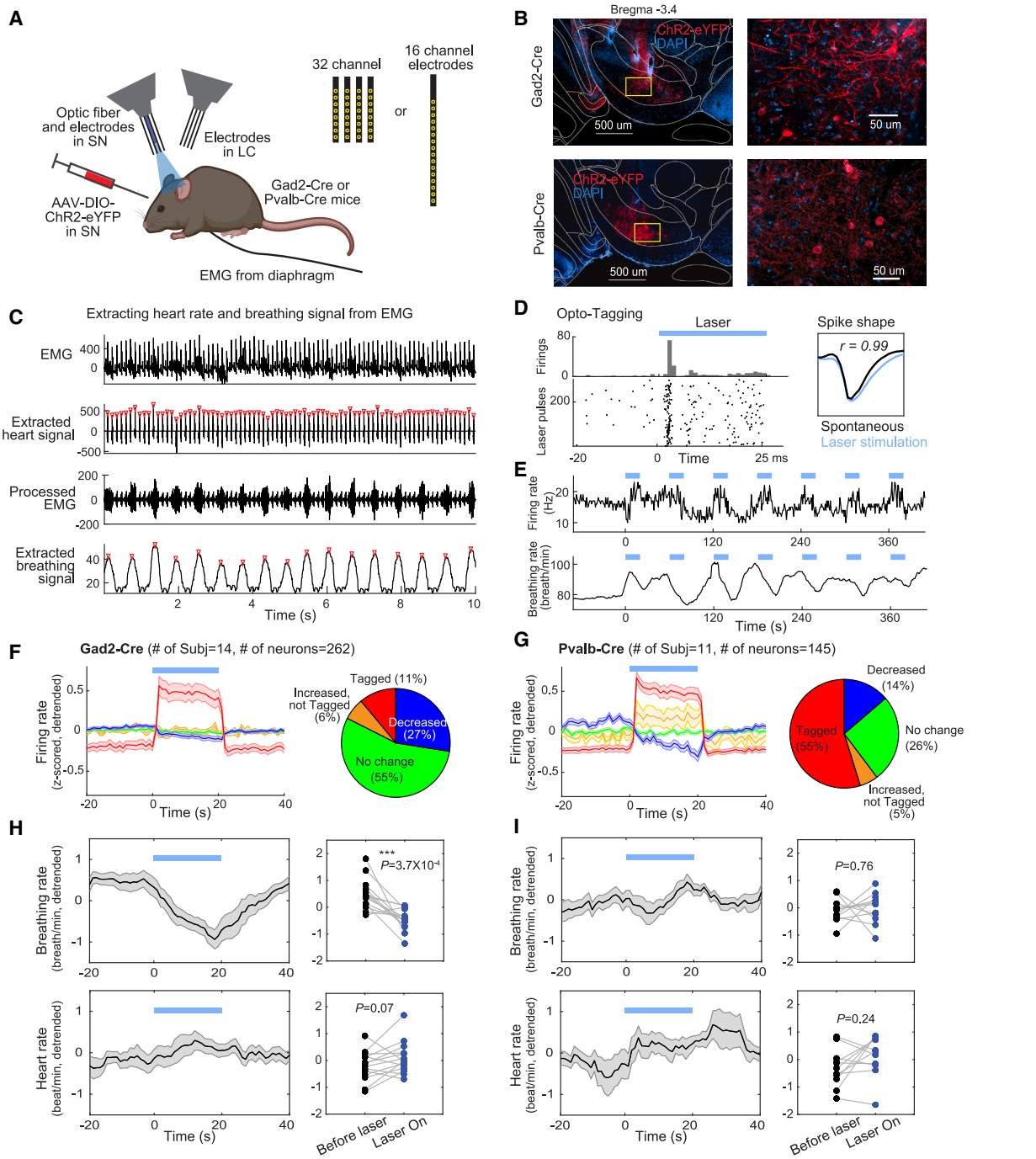

Figure 1. Stimulation of glutamic acid decarboxylase 2 (Gad2)-expressing cells, but not parvalbumin (Pvalb)-expressing cells, in the substantia nigra (SN) decreases breathing rate

(A) Schematic of experimental design. Three weeks after AAV-DIO-ChR2-eYFP virus injection into the SN, the SN was optogenetically stimulated in anesthesized mice using an optic fiber attached to the electrodes. Single unit recordings from SN and locus coeruleus (LC) with diaphragm electromyography (EMG) were obtained simultaneously.

(B) Top left, example of ChR2-eYFP virus expression (red) in a representative Gad2-Cre mouse. Bottom row, example virus expression in a Pvalb-Cre mouse. Enlargements of yellow rectangle regions are shown on the right.

(C) Example heart and breathing rates extracted from the diaphragm EMG signal. EMG raw signal (top row) was thresholded and filtered to obtain the heart signal (second row). This heart signal was then subtracted from the EMG raw signal to obtain a processed EMG signal (third row). A sliding window calculation of standard deviation was applied to the processed EMG signal to obtain the respiratory signal (bottom row). Inverted red triangles indicate individual heartbeats (second row) or breaths (bottom row).

(legend continued on next page)

expression patterns showed that Gad2-expressing cells were located mostly in medial SN, while Pvalb-expressing cells covered broad areas of SN (Figures 1B and S1). Three weeks after Cre-dependent ChR2 virus was injected into the SN, acute electrophysiology was performed with optogenetic stimulation of SN in anesthetized mice (Figure 1A). Optrodes (32- or 16-channel electrodes with optic fiber) targeted SN (Figure S2A), and additional electrodes (32- or 16-channel) were inserted into LC. Electromyography (EMG) from diaphragm muscles was recorded, and this EMG signal was processed to calculate heart and breathing rates with a 10 s sliding window (Figures 1C and S3). Three to five optogenetic stimulation sessions were performed in each subject. For each session, seven consecutive blocks were carried out, where each block consisted of a 20-s laser-on period (10 Hz, 25 ms pulse width, 473 nm wavelength) followed by a 40-s laser-off period.

Optogenetic stimulation of SN was confirmed using single unit recordings in both Gad2-and Pvalb-Cre mice (Figures 1D–1G and S2). A unit was defined as "opto-tagged" if the following two criteria were met: (1) Firing rate increased with laser pulse onset and this increase was highly significant (t-test $p < 0.001$), both within 10 ms of laser pulse onset and over the pulse duration (25ms), compared to the 25ms window before pulse onset; (2) spike shape was similar during laser-on and laser-off periods (correlation coefficient >0.9) (Figure 1D). Units which were not defined as opto-tagged were sub-categorized as having firing rates which increased, decreased, or had no change during a laser pulse (t-test $p < 0.05$, Figures 1F and 1G). The proportions of these various cell types were different between Gad2-Cre and Pvalb-Cre mice, possibly due to the smaller number of cells expressing Gad2 in the SN. The firing activity of the "decreased" units is thought to be suppressed via collateral inhibition received from the opto-tagged units.[32]

During the stimulation of Gad2-expressing cells, breathing rates decreased consistently across mice, then recovered after the stimulation was halted (Figures 1E bottom and 1H top). Stimulation of Pvalb-expressing cells did not have any significant effect on breathing rate (Figure 1I top), showing that the SN's modulatory effects on breathing rate were cell-type specific. No cell type significantly affected heart rate (Figures 1H and 1I bottom).

Stimulation of Gad2-expressing SN cells reduces LC-NA cell firings

We sought to better understand the pathways involved in the modulation of breathing rate by the SN. The LC is known to be involved in vigilance, wakefulness, and breathing control.[27–29] The LC may therefore be a key downstream target in breathing rate control involving the SN. To investigate this, we examined the firings of LC cells during SN cell stimulation.

Previous literature has reported that noradrenergic (NA) cells in the LC are characterized by low firing rates, longer spike width, and reduced firing rates with adrenergic agonist, whereas the GABAergic cells adjacent to the LC are known to have higher firing rates and shorter spike widths.[28,33,34] Recorded units in the LC (Figure 2A) were categorized into putative NA, putative GABA, and non-categorized cells based on spike width, firing rate, and response to the adrenergic agonist dexmedetomidine (Figures 2C and 2D).

The firing rates of putative NA cells correlated with breathing rate (Figures 2B and S4B) and decreased significantly when Gad2-expressing SN cells were stimulated (Figure 2E). The putative GABAergic cells or non-categorized cells from the Gad2-Cre mice showed marginal decrease or no change in firing rate, respectively. No cell types from Pvalb-Cre mice showed significant changes, consistent with their lack of effect on breathing rate (Figure 2F).

The breathing rate reduction caused by stimulation of Gad2-expressing SN cells was not perfectly consistent, even in a given subject. We hypothesized that this was due to variations in baseline NA cell activity, i.e., the NA cells need to be active to be able to relay information. To investigate the relationship between breathing rate reduction and baseline NA cell activity, we compared the NA cell firing rates between blocks with and without breathing rate reduction (Figure 2G). The blocks with decreasing breathing rate had elevated baseline firing rates of NA cells. This was not observed in other cell types (Figure 2H). These results show that SN reduction of breathing rate is only effective when NA cell firing rates are relatively high. This suggests that inhibitory inputs from SN to LC are not effective when the NA cell firing rates are already too low.

Dexmedetomidine suppresses SN's effect on breathing rate via LC

Dexmedetomidine is a selective adrenergic alpha-2 agonist which is commonly used for sedation, and is known to control arousal by reducing the activity of NA cells in LC.[35,36] To further demonstrate that breathing rate control by the SN is dependent on the NA cells, we injected dexmedetomidine prior to SN cell stimulation (Figure 3A). Under the presence of dexmedetomidine, overall firing rates of LC cells were reduced (Figures 2C,

(D) Example of a unit defined as "opto-tagged". Firing histogram (top left) and spike raster plot (bottom left) show increased firing with the laser pulse. Spike shapes during laser stimulation and spontaneous firing (right) show strong temporal correlation (Pearson's correlation).
(E) Example SN Gad2-expressing cell firing rates (top graph) and breathing rates (bottom graph) measured during laser block design (7 cycles of 20 s on, 40s off). The light blue bars indicate 20 s laser-on stimulation periods. The bottom plot shows breathing rate decreasing during laser stimulations.
(F) Firing rate time courses of Gad2-Cre mice averaged over 60s stimulation blocks (left). The shaded area indicates ±S.E.M. across neurons. Pie chart shows percent of units categorized by their firing rate changes in response to the laser pulse (right). The line graph (left) shows response to the laser blocks and the cell categorization (right) was based on the response to each laser pulse.
(G) Same as (F) for Pvalb-Cre mice.
(H) Left, Plots show change in breathing rate (top row) or change in heart rate (bottom row), averaged over all stimulation blocks in Gad2-Cre mice. The shaded area indicates ±S.E.M. across subjects. Right, Before (20s) and during (20s) laser stimulation paired plots show the change in breathing rate or heart rate for each Gad2-Cre mouse. Gad2-Cre mice show significant breathing rate reductions with laser stimulation (two-sided Wilcoxon signed rank test, $^{***}p < 0.001$).
(I) Same as (H) for Pvalb-Cre mice; however, they show no significant respiratory changes.
(E–I) 20 s laser-on periods (10 Hz, 25 ms on, 75 ms off) are indicated by the light blue bar.

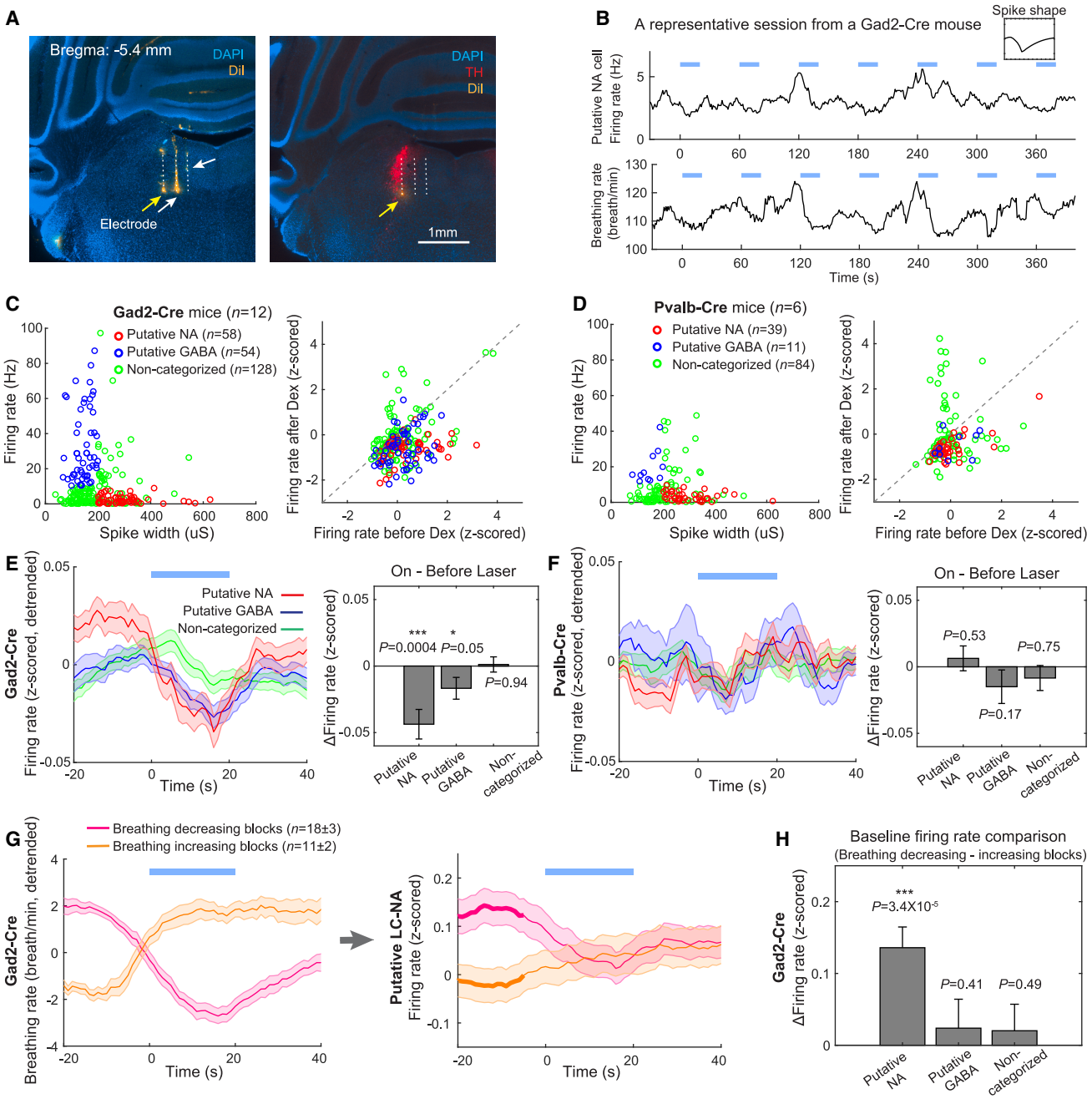

Figure 2. Stimulation of Gad2-expressing cells in the SN decreases the firing rate of LC-norardrenaline (NA) cells

(A) Example histology images of two consecutive brain slices showing electrode tracks (DiI orange stain) in the LC. LC was visualized using tyrosine hydroxylase (TH)-immunolabeling (red stain on right panel). The electrode targeting the LC is indicated by the yellow arrow.

(B) Decrease in firing rate in an example putative NA cell (top row) during block design laser stimulation of SN, with corresponding breathing rate (bottom row). Each blue horizontal bar indicates 20 s laser-on SN Gad2 stimulation period. Inset shows spike shape.

(C) Categorization of cells by firing rate and spike width (left), with response to dexmedetomidine (Dex, right) from Gad2-Cre mice (n = 12). The scatterplot shows units' firing rates averaged 60 s before, and 40–100 s after, Dex injection.

(D) Same format as (C) for Pvalb-Cre mice (n = 6).

(E) Z-scored, detrended firing rates averaged over laser blocks, measured in Gad2-Cre mice. Shaded area indicates S.E.M. across neurons in each group. Bar graphs show average firing rate over the 20 s of laser stimulation, minus the average firing rate over 20 s before the laser. The firing rates of putative NA cells decreased significantly with Gad2-expressing SN cell stimulation (mean ± S.E.M. over neurons, two-sided Wilcoxon signed rank test, ***$p < 0.001$, *$p < 0.05$).

(F) Same format as in (E) for Pvalb-Cre mice. No cell type showed changes with laser stimulation.

(legend continued on next page)

2D, and S4A), and laser stimulation of Gad2-expressing cells had no effect on breathing rate (Figure 3C). This indicates that the effect of SN on breathing rate is interrupted by dexmedetomidine inhibition of NA cells (Figure 3B). Due to the reduced baseline firing rates of putative NA cells, the firing rates remained unchanged during laser stimulation of Gad2-expressing cells (Figure 3E). Interestingly, the firing rates of putative GABAergic cells were decreased during laser stimulation of SN Gad2-expressing cells. After dexmedetomidine injection, laser stimulation of Pvalb-expressing cells had no significant effect on breathing rate, heart rate, or neuronal firing rate, as expected (Figures 3D and 3F).

CO_2 exposure suppresses SN's effect on breathing rate

Respiration regulates blood pCO_2 using feedback from chemoreceptors in multiple central and peripheral areas (Figure 4B) which detect changes in CO_2 and pH.[21,23] It has been suggested that the LC is one of these chemoreceptors because the LC cells have been shown to increase firing rate in response to hypercapnia in a dose dependent manner.[30,31,37]

To investigate whether SN breathing rate control is maintained during hypercapnia, we exposed mice to 7% CO_2 during the SN cell stimulation (Figures 4A and S4A). Under these conditions, we hypothesized that SN's control would be attenuated due to a stronger, compensatory response of chemoreceptors registering persistent elevated CO_2. As expected, stimulation of Gad2-expressing SN cells under 7% CO_2 had no effect on breathing rate (Figure 4C), suggesting that critical respiratory need overrides SN's control over breathing. Interestingly, the inhibition effect on the putaitve NA cells was still present (Figure 4E), further suggesting that hypercapnia triggers other chemosensitive regions to maintain essential respiration regardless of SN inputs to LC. These data show that critical respiratory need can decouple some LC cell firings from breathing rate (Figure S4B). Under 7% CO2, laser stimulation of Pvalb-expressing cells had no significant effect on breathing rate, heart rate, or NA cell firing rate, as expected (Figures 4D and 4F).

Direct stimulation of LC increases breathing rate

It has been shown that pharmacological activation of LC increases breathing rate in freely moving mice.[25] We further tested if direct stimulation of LC leads to breathing rate increase in anesthetized mice. To target LC-NA cells specifically, we used dopamine-β-hydroxylase (Dbh)-Cre mice (n = 10) and injected Cre-dependent ChrimsonR virus into the LC. Eight out of these ten mice showed virus expression localized to LC (Figure 5B), and the other two mice were excluded from analysis. Three weeks after virus injection, acute LC electrophysiology and EMG diaphragm measurements were performed in anesthetized mice during block paradigm red laser (638nm) stimulation of Dbh-expressing LC cells (Figure 5A). As expected, optogenetic stimulation of Dbh-expressing LC cells increased breathing rate (Figures 5C and 5D). Histology images showed that the electrodes had targeted the LC in 6 mice (e.g., Figure 5B). LC units from these mice were labeled as "opto-tagged" if the laser pulse increased firing rate without changes in spike shape (as defined for SN opto-tagged cells) (Figure 5D). We also verified that opto-tagged units matched the categorization of putative NA cells (Figure 5E). Opto-tagged units mainly overlapped with putative NA cells and did not overlap with putative GABAergic cells, showing that our categorization was accurate.

DISCUSSION

In this study, we demonstrate the significant role of GABAergic neurons in the SN in the modulation of breathing rate. Specifically, we found that stimulation of Gad2-expressing cells in the output of the basal ganglia (SN) modulates breathing rate in a manner which depends on baseline firing rates of NA cells in the LC. These data strongly suggest the existence of a previously unknown respiratory control circuit which passes from the SN to the LC (SN-LC). The LC is known to regulate arousal and is involved in sleep, emotion, attention, feeding, and memory.[29,38–42] The SN-LC circuit therefore has multiple potential functional implications. This circuit could be related to the reported role of Gad2-expressing SN cells in sleep control.[12] The inhibition of LC firings by SN could reduce arousal levels, inducing sleep with accompanying breathing rate reduction.[43,44] The SN-LC circuit could also be involved in limbic system control. It has been suggested that the basal ganglia has parallel circuits of limbic, associative, and motor control that are spatially segregated into medial, middle and lateral SN, respectively.[45–47] The location of Gad2-expressing SN cells in our experiments was mostly medial, indicating that these cells may be part of the limbic circuit. The LC is critically involved in emotional processes, and breathing rate is tightly coupled with emotional arousal.[22,48] The SN-LC circuit may therefore be involved in the control of emotions, with breathing rate as a closely linked indicator of emotional arousal. Future studies of the SN-LC circuit during different emotional states would shed light on this possibility.

We further identified direct axonal inputs from GABAergic neurons in both the SNr and SNc to the LC using retrograde tracing experiments (Figure S5). We injected retrobeads into the LC and confirmed colocalization with Gad2-expressing neurons in the SN. This finding provides direct evidence supporting the Gad2-expressing GABAergic projections from SN to LC-NA neurons, consistent with a previous finding suggesting direct connections

(G) To investigate the relationship between breathing rate change and baseline firing rate of NA cells in the Gad2-Cre mice, laser blocks (60 s time window) were categorized as having "Increasing" or "Decreasing" breathing rates during laser stimulation (left graph, n indicates mean ± S.E.M. of numbers of blocks for each subject, and shaded area indicates ±S.E.M. across subjects). Z-scored firing rate time courses for putative NA cells were averaged over each block type (right graph, shaded area indicates ±S.E.M. across neurons). The blocks with breathing rate decrease show elevated baseline firing rates of putative NA cells. Thicker lines indicate significant difference between the two subdivided blocks (two-sided Wilcoxon signed rank test, Bonferroni corrected with the number of 5-s time windows, $p < 0.05$).

(H) Difference in baseline firing rate for each of the cell categories defined in (C) (mean ± S.E.M. over neurons, two-sided Wilcoxon signed rank test, $^{***}p < 0.001$). Only putative NA cells showed elevated baseline firing rate in the block where respiration was modulation by Gad2-expressing SN cells.

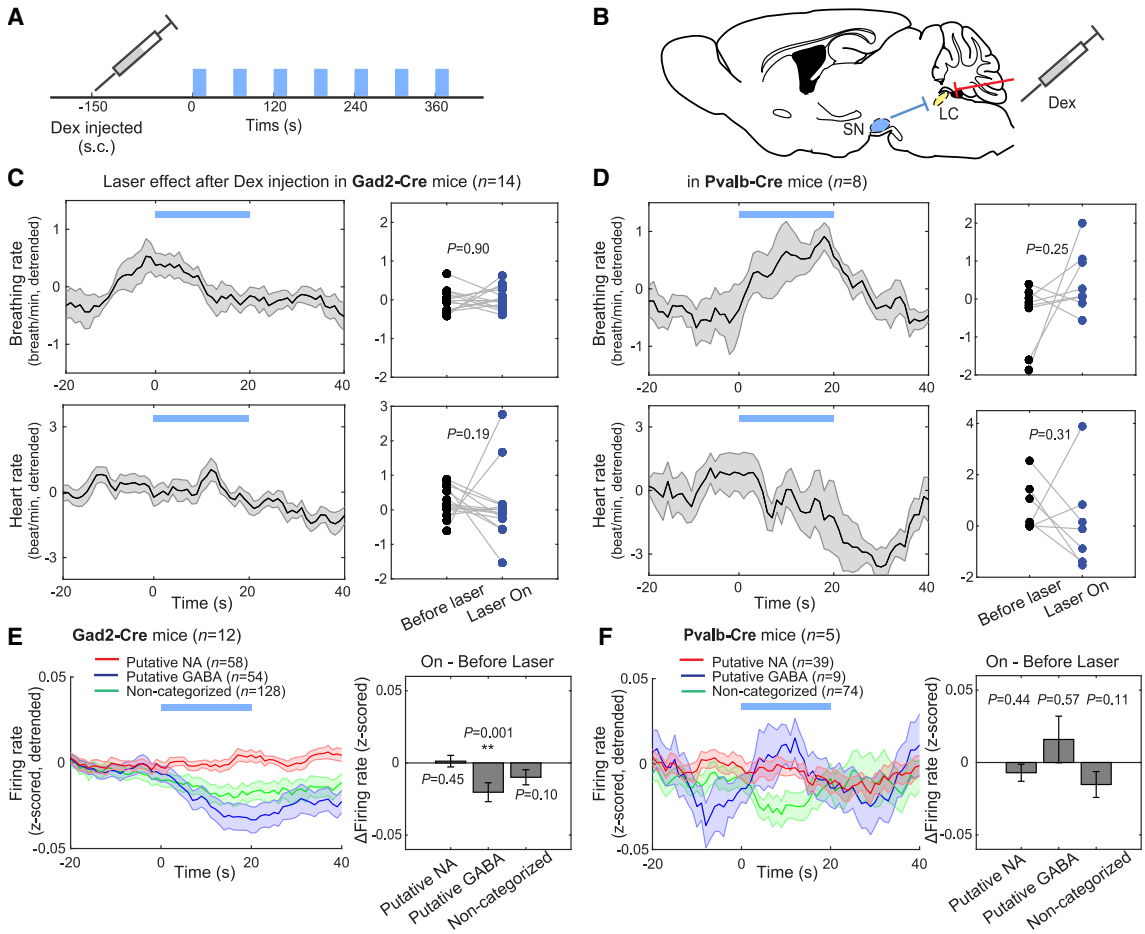

Figure 3. Dexmedetomidine (Dex) suppresses the decrease in breathing rate driven by stimulation of Gad2-expressing cells in SN

(A) Schematic of experimental design. Same experiment setup as in Figure 1A, but with Dex injection.

(B) Illustration of circuits. Dex is known to inhibit NA cells, thus inhibitory inputs from SN would not be effective if the NA cells were already strongly inhibited.

(C and D) Breathing rate and heart rate do not show any significant change with stimulation of SN in the Gad2-Cre (C) or Pvalb-Cre (D) mice. Same format as in Figure 1H.

(E and F) Putative NA cells show no significant change in firing rate with stimulation of SN cells in Gad2-Cre (E) or Pvalb-Cre (F) mice because they are already inhibited by Dex. Same format as in the Figure 2E (two-sided Wilcoxon signed rank test, $^{**}p < 0.01$).

between these regions.[12] Our experiments demonstrate that these inputs likely contribute to both the modulation of LC activity and breathing rate, reinforcing the idea that the SN exerts a significant influence over LC-mediated physiological processes.

However, it remains unclear whether projections from the SN to the LC are the sole source of this modulatory control, and it is important to note that these neurons also send diffuse projections to other downstream targets. In particular, we recognize that other multi-synaptic pathways—such as those involving the pre-Bötzinger complex (preBotC), mesencephalic locomotor region (MLR), and periaqueductal gray matter (PAG)—may play complementary roles in linking SN activity with LC-mediated breathing rate control. The preBotC has been reported to receive inputs from the SN and send outputs to the LC.[22,25,26,49,50] However, based on the delayed nature of the breathing rate modulation we observed, it is unlikely that direct GABAergic projections from SN to preBotC are responsible for the effects on breathing rate, as direct GABAergic input to preBotC would typically result in a more immediate and potent modulation of respiratory activity. Moreover, previous studies have shown that projections from SN to preBotC, while present, are comparatively weak and may not be the primary mechanism in this instance.[26]

The MLR also directly receives inputs from the SN and projects to preBötC.[51,52] Recent studies suggest that MLR stimulation can increase breathing rate frequency during physical activity,[52] linking it to breathing modulation during exercise. The disinhibition of MLR cells by Gad2-expressing SN neurons may contribute to locomotion-related breathing modulation. Similarly, the PAG receives direct input from the SN and is closely connected with the LC, playing a role in breathing rate control, particularly in response to emotional or stress-related stimuli.[22,53,54] These multi-synaptic routes, via either the MLR or PAG, may therefore mediate SN's influence on LC activity and breathing regulation, especially in the case of delayed breathing

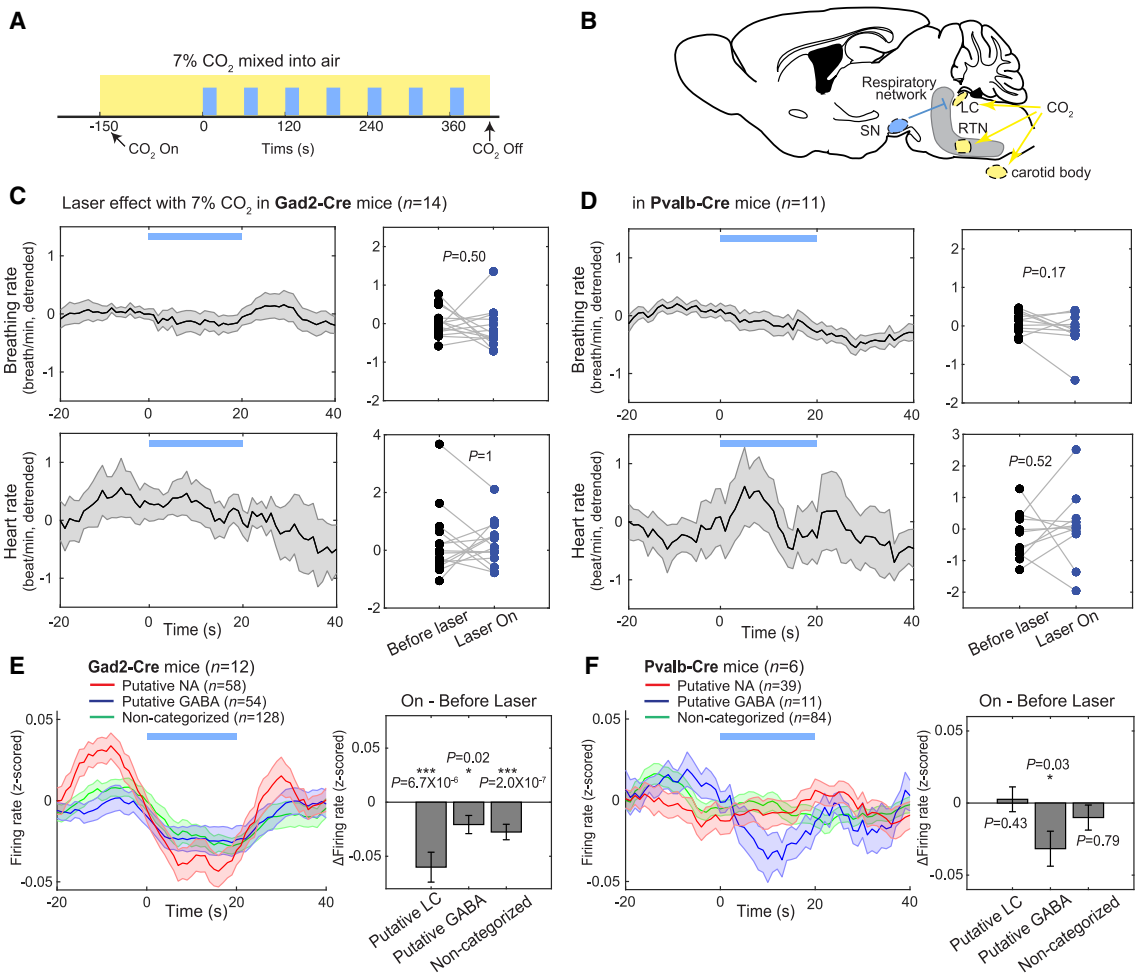

Figure 4. Increasing the CO_2 level from less than 1%–7% suppresses the decrease in breathing rate driven by stimulation of Gad2-expressing cells in the SN

(A) Schematic of experimental design. Yellow shaded area indicates period of CO_2 exposure (hypercapnia).

(B) Illustration of circuits known to be related to chemosensitivity.

(C and D) Under high CO_2 presence, breathing rate and heart rate do not show any significant change with stimulation of SN in Gad2-Cre mice (C) or Pvalb-Cre mice (D). Same format as in Figure 1H.

(E) Under high CO_2 presence, Gad2-expressing SN cell stimulation results in significantly decreased firing rate for all LC cell types in Gad2-Cre mice (n = 12). This finding shows that hypercapnia overrides SN cell influence on breathing. Same format as Figure 2E.

(F) Results for Pvalb-Cre mice, same format as (E) (n = 6).

rate modulation. Future studies that precisely map these downstream connections will be important to further elucidate the role of the SN in breathing rate control and the potential contribution of multi-synaptic circuits.

We focused on Pvalb- and Gad2-expressing neurons in the SN due to their distinct anatomical locations and functional roles in inhibitory signaling.[12] Although some studies suggest co-expression between Gad2 and Pvalb neurons,[11,55] these populations are anatomically segregated within the SN, with Pvalb neurons primarily located dorsally and Gad2 neurons more medially.[12] This anatomical separation underpins their functional divergence, which was central to our study. While molecular overlap may exist, our experimental design focused on the distinct roles these populations play in SN-mediated control of respiratory circuits.

In our study, we targeted Gad2-expressing neurons in the SN with ChR2 injections. However, one possible concern is that due to the proximity of the midbrain reticular nucleus (MRN) to the SN, some Gad2-expressing MRN neurons could have been inadvertently activated during SN stimulation. Our retrobead tracing experiments from the LC revealed sparse labeling of retrobeads in the MRN (Figure S5). Importantly, there is very little colocalization of retrobeads with Gad2-expressing neurons, suggesting that inadvertent MRN activation is unlikely to have contributed to the observed modulation of breathing rate in our study. Given these considerations, we conclude that there was

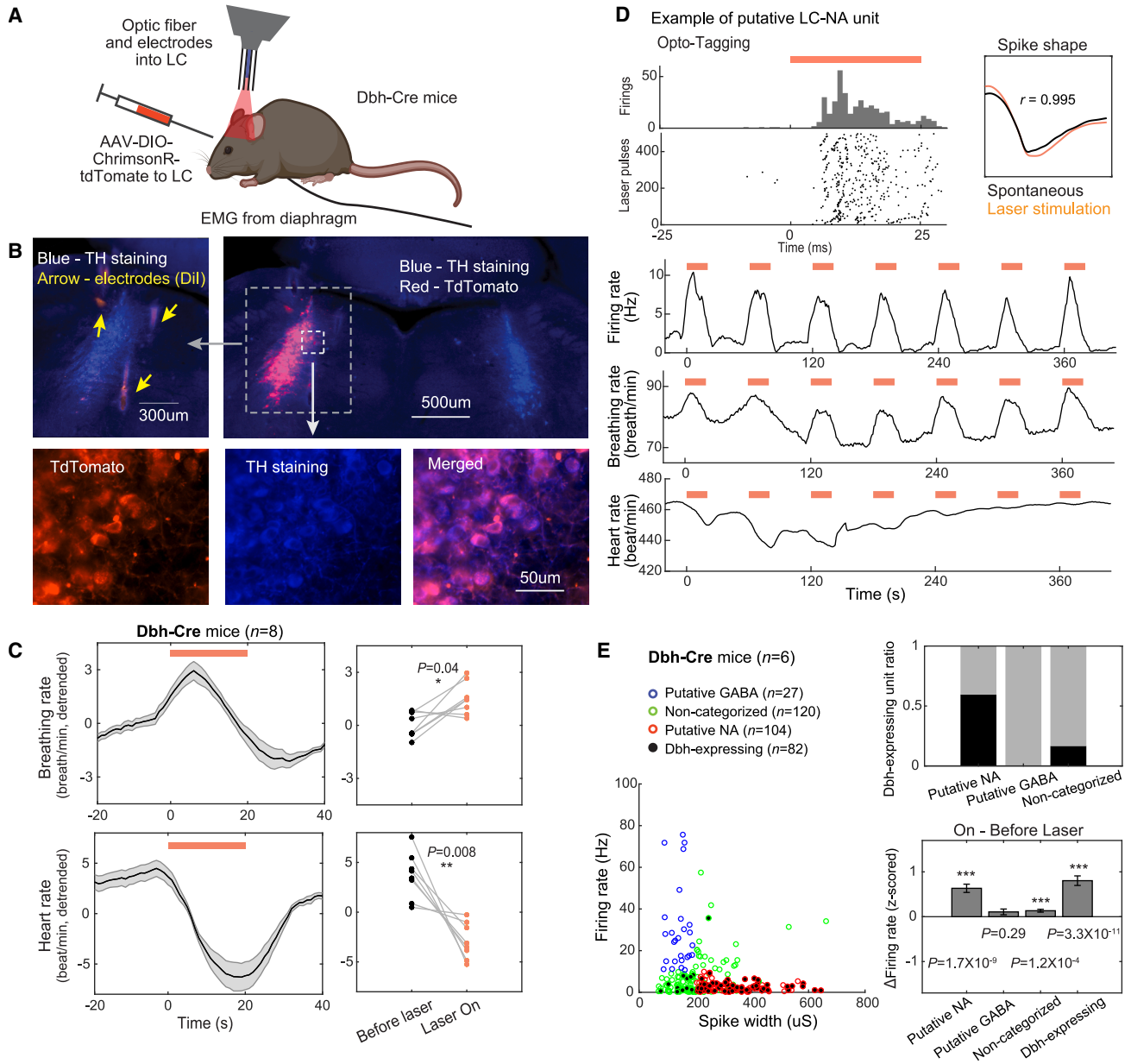

Figure 5. Direct stimulation of NA cells in LC increases breathing rate

(A) Schematic of experimental design. Three weeks after ChrimsonR virus was injected into the LC of dopamine-β-hydroxylase (Dbh)-Cre mice, mice were anesthetized and the LC was optogenetically stimulated using an optic fiber attached to electrodes. Signals from LC and diaphragm EMG were recorded simultaneously.

(B) Top left, DiI-stained electrodes are shown targeting the LC in this coronal section. Top right and bottom, virus expression (TdTomato) is shown to be localized to the LC cells labeled with TH immunostaining.

(C) Laser stimulation of LC increases breathing rate and decreases heart rate in Dbh-Cre mice. Same format as in Figure 1H (two-sided Wilcoxon signed rank test, $^{**}p < 0.01$, $^{*}p < 0.05$).

(D) An opto-tagging example of a Dbh-expressing unit. Top left, spike rastergram shows strong increase in firing rate with laser stimulation (orange). Top right, spike shape during laser (orange) is highly correlated with spontaneous (black) spike shape (Pearson's correlation). Bottom, firing rates and breathing rates show increase with laser stimulation.

(E) Left, spike width versus firing rate for categorized cells (same criteria as in Figure 2C) from six mice. Also plotted are Dbh-expressing cells which were identified as opto-tagged (black). Right top, fraction of categorized cells which were identified as opto-tagged Dbh-expressing cells (black sections). This fraction was largest for putative NA cells, showing that the putative NA categorization reasonably represents the Dbh-expressing cells. Bottom right, average firing rate differences between On Laser and Before Laser, for each cell group (mean ± S.E.M. over neurons, two-sided Wilcoxon signed rank test, $^{***}p < 0.001$).

no significant influence of MRN activation on our results, and the primary effects were mediated by the SN.

Chemosensitivity, which refers to detection of changes in CO_2/H^+ in the body with reactive modulation of respiration, is critical to the survival of organisms.[23] Under the threatening condition of high CO_2 (hypercapnic state), we show that SN stimulation still inhibits LC-NA cells but no longer affects breathing rate. This decoupling of breathing rate from NA cell activity suggests that there are other respiratory control mechanisms which dominate during hypercapnia. Although the LC has been suggested as a vigilance center equipped with chemoreceptors, there are multiple other known chemoreceptors such as the carotid body, the retrotrapezoid nucleus (RTN), and serotonergic neurons.[21,56] Among those, RTN is known as a critical central chemoreceptor and sends direct inputs to respiratory pattern generators.[57] Serotonergic neurons are also reported to be important chemoreceptors, with high sensitivity to CO_2 levels.[58] With multiple brain areas functioning as chemoreceptors, our current data indicate a limited modulatory role of the SN-LC circuit during hypercapnia. It should be noted that the 7% CO_2 employed in our study is a strong hypercapnic stimulus, although it has been used in many previous rodent studies of breathing dynamics.[14,18,24,30] In future work, it would be interesting to determine the minimum level of hypercapnia required to decouple NA cell activity from breathing rate, to improve our understanding of the relationship between the SN-LC pathway and other breathing control circuits.

Limitations of the study

Our stimulation procedures were performed under anesthesia in mice to exclude potential indirect effects related to locomotor activity or emotional states. However, this approach leaves the possibility that the Gad2-SN cells may serve a different function in awake behaving or naturally sleeping mice. Future studies in mice without anesthesia would be important to further elucidate the role of the SN-LC circuit.

In addition, we cannot completely exclude the possibility that the Alpha2 agonist dexmedetomidine used in our pharmacology experiments may have affected regions outside the LC. However, the observed respiratory effects were critically dependent on LC activities, as evidenced by the direct stimulation of LC neurons and the effect of LC-NA baseline firing rates.

Our study targeted both SNr and SNc GABAergic cells due to their close proximity. The function of SNc GABAergic cells is not clearly known, but these cells may inhibit nearby SNc dopmainegic cells, which could potentially modulate respiration. However, this effect is unlikely to be critical, as direct optogentic stimulation of Pvalb-expressing SN cells had no consistent effect on breathing rate, despite the known inhibitory inputs to SNc dopaminergic cells.[8]

RESOURCE AVAILABILITY

Lead contact

Further information and any requests should be directed to and will be fulfilled by the lead contact, Jin Hyung Lee (ljinhy@stanford.edu).

Materials availability

This study did not generate new unique materials or reagents.

Data and code availability

- All data reported in this paper will be shared by the lead contact upon reasonable request.
- This paper does not report original code.
- Any additional information required to reanalyze the data reported in this paper is available from the lead contact upon request.

STAR★METHODS

Detailed methods are provided in the online version of this paper and include the following:

- KEY RESOURCES TABLE
- EXPERIMENTAL MODEL AND SUBJECT DETAILS
  - Subjects
- METHOD DETAILS
  - Virus injections and stereotaxic surgery
  - Acute electrophysiology with optogenetics
  - Laser stimulation of SN in Gad2-Cre or Pvalb-Cre mice
  - Laser stimulation of LC in Dbh-Cre mice
  - Retrograde tracing studies
  - Histology and immunofluorescence
- QUANTIFICATION AND STATISTICAL ANALYSIS
  - Breathing and heart rate analysis
  - Electrophysiological data analysis

ACKNOWLEDGMENTS

This work was supported by NIH/NIMH RF1 MH114227 and NIH/NINDS DP1 NS116783. The authors would also like to acknowledge Benjamin Liu for his contribution in editing the manuscript.

AUTHOR CONTRIBUTIONS

B.G.: Conceptualization, methodology, software, formal analysis, investigation, data curation, writing–original draft, and visualization; J.G.K.: writing–review and editing, investigation, and data curation; G.O.C.: writing–review and editing; A.H.: formal analysis and investigation; J.H.L.: conceptualization, metholology, investiation, data curation, writing–review and editing, supervision, project administration, and funding acquisition.

DECLARATION OF INTERESTS

J.H.L. is a founder, shareholder, and consultant for LVIS, a private company which develops neural information analysis technology.

SUPPLEMENTAL INFORMATION

Supplemental information can be found online at https://doi.org/10.1016/j.isci.2025.112423.

Received: May 22, 2023
Revised: February 4, 2025
Accepted: April 9, 2025
Published: April 14, 2025

REFERENCES

1. Deniau, J.M., Mailly, P., Maurice, N., and Charpier, S. (2007). The pars reticulata of the substantia nigra: a window to basal ganglia output. Prog. Brain Res. *160*, 151–172. https://doi.org/10.1016/S0079-6123(06)60009-5.
2. Gu, B.M., and Berke, J.D. (2022). Altered basal ganglia output during self-restraint. Elife *11*, e82143. https://doi.org/10.7554/eLife.82143.

3. Schmidt, R., Leventhal, D.K., Mallet, N., Chen, F., and Berke, J.D. (2013). Canceling actions involves a race between basal ganglia pathways. Nat. Neurosci. *16*, 1118–1124. https://doi.org/10.1038/nn.3456.

4. Kim, H.F., Amita, H., and Hikosaka, O. (2017). Indirect Pathway of Caudal Basal Ganglia for Rejection of Valueless Visual Objects. Neuron *94*, 920–930.e3. https://doi.org/10.1016/j.neuron.2017.04.033.

5. Fan, D., Rossi, M.A., and Yin, H.H. (2012). Mechanisms of action selection and timing in substantia nigra neurons. J. Neurosci. *32*, 5534–5548. https://doi.org/10.1523/JNEUROSCI.5924-11.2012.

6. Ding, L., and Gold, J.I. (2013). The basal ganglia's contributions to perceptual decision making. Neuron *79*, 640–649. https://doi.org/10.1016/j.neuron.2013.07.042.

7. Klaus, A., Alves da Silva, J., and Costa, R.M. (2019). What, If, and When to Move: Basal Ganglia Circuits and Self-Paced Action Initiation. Annu. Rev. Neurosci. *42*, 459–483. https://doi.org/10.1146/annurev-neuro-072116-031033.

8. Rizzi, G., and Tan, K.R. (2019). Synergistic Nigral Output Pathways Shape Movement. Cell Rep. *27*, 2184–2198.e4. https://doi.org/10.1016/j.celrep.2019.04.068.

9. Foster, N.N., Barry, J., Korobkova, L., Garcia, L., Gao, L., Becerra, M., Sherafat, Y., Peng, B., Li, X., Choi, J.H., et al. (2021). The mouse cortico-basal ganglia-thalamic network. Nature *598*, 188–194. https://doi.org/10.1038/s41586-021-03993-3.

10. Liu, P., and Basso, M.A. (2008). Substantia nigra stimulation influences monkey superior colliculus neuronal activity bilaterally. J. Neurophysiol. *100*, 1098–1112. https://doi.org/10.1152/jn.01043.2007.

11. McElvain, L.E., Chen, Y., Moore, J.D., Brigidi, G.S., Bloodgood, B.L., Lim, B.K., Costa, R.M., and Kleinfeld, D. (2021). Specific populations of basal ganglia output neurons target distinct brain stem areas while collateralizing throughout the diencephalon. Neuron *109*, 1721–1738.e4. https://doi.org/10.1016/j.neuron.2021.03.017.

12. Liu, D., Li, W., Ma, C., Zheng, W., Yao, Y., Tso, C.F., Zhong, P., Chen, X., Song, J.H., Choi, W., et al. (2020). A common hub for sleep and motor control in the substantia nigra. Science *367*, 440–445. https://doi.org/10.1126/science.aaz0956.

13. McGregor, M.M., and Nelson, A.B. (2019). Circuit Mechanisms of Parkinson's Disease. Neuron *101*, 1042–1056. https://doi.org/10.1016/j.neuron.2019.03.004.

14. Aquino, Y.C., Cabral, L.M., Miranda, N.C., Naccarato, M.C., Falquetto, B., Moreira, T.S., and Takakura, A.C. (2022). Respiratory disorders of Parkinson's disease. J. Neurophysiol. *127*, 1–15. https://doi.org/10.1152/jn.00363.2021.

15. Mehanna, R., and Jankovic, J. (2010). Respiratory problems in neurologic movement disorders. Parkinsonism Relat. Disord. *16*, 628–638. https://doi.org/10.1016/j.parkreldis.2010.07.004.

16. Zhang, L.Y., Liu, W.Y., Kang, W.Y., Yang, Q., Wang, X.Y., Ding, J.Q., Chen, S.D., and Liu, J. (2016). Association of rapid eye movement sleep behavior disorder with sleep-disordered breathing in Parkinson's disease. Sleep Med. *20*, 110–115. https://doi.org/10.1016/j.sleep.2015.12.018.

17. Andrzejewski, K., Budzińska, K., and Kaczyńska, K. (2019). Effect of 6-OHDA on hypercapnic ventilatory response in the rat model of Parkinson's disease. Physiol. Res. *68*, 285–293. https://doi.org/10.33549/physiolres.933949.

18. Tuppy, M., Barna, B.F., Alves-Dos-Santos, L., Britto, L.R.G., Chiavegatto, S., Moreira, T.S., and Takakura, A.C. (2015). Respiratory deficits in a rat model of Parkinson's disease. Neuroscience *297*, 194–204. https://doi.org/10.1016/j.neuroscience.2015.03.048.

19. Angyán, L. (1994). Somatomotor and cardiorespiratory responses to basal ganglia stimulation in cats. Physiol. Behav. *56*, 167–173. https://doi.org/10.1016/0031-9384(94)90275-5.

20. Smith, J.C. (2022). Respiratory rhythm and pattern generation: Brainstem cellular and circuit mechanisms. Handb. Clin. Neurol. *188*, 1–35. https://doi.org/10.1016/B978-0-323-91534-2.00004-7.

21. Guyenet, P.G., and Bayliss, D.A. (2022). Central respiratory chemoreception. Handb. Clin. Neurol. *188*, 37–72. https://doi.org/10.1016/B978-0-323-91534-2.00007-2.

22. Ashhad, S., Kam, K., Del Negro, C.A., and Feldman, J.L. (2022). Breathing Rhythm and Pattern and Their Influence on Emotion. Annu. Rev. Neurosci. *45*, 223–247. https://doi.org/10.1146/annurev-neuro-090121-014424.

23. Guyenet, P.G., and Bayliss, D.A. (2015). Neural Control of Breathing and CO2 Homeostasis. Neuron *87*, 946–961. https://doi.org/10.1016/j.neuron.2015.08.001.

24. Depuy, S.D., Kanbar, R., Coates, M.B., Stornetta, R.L., and Guyenet, P.G. (2011). Control of breathing by raphe obscurus serotonergic neurons in mice. J. Neurosci. *31*, 1981–1990. https://doi.org/10.1523/JNEUROSCI.4639-10.2011.

25. Liu, N., Fu, C., Yu, H., Wang, Y., Shi, L., Hao, Y., Yuan, F., Zhang, X., and Wang, S. (2021). Respiratory Control by Phox2b-expressing Neurons in a Locus Coeruleus-preBotzinger Complex Circuit. Neurosci. Bull. *37*, 31–44. https://doi.org/10.1007/s12264-020-00519-1.

26. Yang, C.F., Kim, E.J., Callaway, E.M., and Feldman, J.L. (2020). Monosynaptic Projections to Excitatory and Inhibitory preBotzinger Complex Neurons. Front. Neuroanat. *14*, 58. https://doi.org/10.3389/fnana.2020.00058.

27. Guyenet, P.G., Koshiya, N., Huangfu, D., Verberne, A.J., and Riley, T.A. (1993). Central respiratory control of A5 and A6 pontine noradrenergic neurons. Am. J. Physiol. *264*, R1035–R1044. https://doi.org/10.1152/ajpregu.1993.264.6.R1035.

28. Breton-Provencher, V., and Sur, M. (2019). Active control of arousal by a locus coeruleus GABAergic circuit. Nat. Neurosci. *22*, 218–228. https://doi.org/10.1038/s41593-018-0305-z.

29. Carter, M.E., Yizhar, O., Chikahisa, S., Nguyen, H., Adamantidis, A., Nishino, S., Deisseroth, K., and de Lecea, L. (2010). Tuning arousal with optogenetic modulation of locus coeruleus neurons. Nat. Neurosci. *13*, 1526–1533. https://doi.org/10.1038/nn.2682.

30. Gargaglioni, L.H., Hartzler, L.K., and Putnam, R.W. (2010). The locus coeruleus and central chemosensitivity. Respir. Physiol. Neurobiol. *173*, 264–273. https://doi.org/10.1016/j.resp.2010.04.024.

31. Magalhaes, K.S., Spiller, P.F., da Silva, M.P., Kuntze, L.B., Paton, J.F.R., Machado, B.H., and Moraes, D.J.A. (2018). Locus Coeruleus as a vigilance centre for active inspiration and expiration in rats. Sci. Rep. *8*, 15654. https://doi.org/10.1038/s41598-018-34047-w.

32. Brown, J., Pan, W.X., and Dudman, J.T. (2014). The inhibitory microcircuit of the substantia nigra provides feedback gain control of the basal ganglia output. Elife *3*, e02397. https://doi.org/10.7554/eLife.02397.

33. Bornert, P., and Bouret, S. (2021). Locus coeruleus neurons encode the subjective difficulty of triggering and executing actions. PLoS Biol. *19*, e3001487. https://doi.org/10.1371/journal.pbio.3001487.

34. Kalwani, R.M., Joshi, S., and Gold, J.I. (2014). Phasic activation of individual neurons in the locus ceruleus/subceruleus complex of monkeys reflects rewarded decisions to go but not stop. J. Neurosci. *34*, 13656–13669. https://doi.org/10.1523/JNEUROSCI.2566-14.2014.

35. Jorm, C.M., and Stamford, J.A. (1993). Actions of the hypnotic anaesthetic, dexmedetomidine, on noradrenaline release and cell firing in rat locus coeruleus slices. Br. J. Anaesth. *71*, 447–449. https://doi.org/10.1093/bja/71.3.447.

36. Chiu, T.H., Chen, M.J., Yang, Y.R., Yang, J.J., and Tang, F.I. (1995). Action of dexmedetomidine on rat locus coeruleus neurones: intracellular recording in vitro. Eur. J. Pharmacol. *285*, 261–268. https://doi.org/10.1016/0014-2999(95)00417-j.

37. Pineda, J., and Aghajanian, G.K. (1997). Carbon dioxide regulates the tonic activity of locus coeruleus neurons by modulating a proton- and polyamine-sensitive inward rectifier potassium current. Neuroscience *77*, 723–743. https://doi.org/10.1016/s0306-4522(96)00485-x.

38. Totah, N.K.B., Logothetis, N.K., and Eschenko, O. (2019). Noradrenergic ensemble-based modulation of cognition over multiple timescales. Brain Res. *1709*, 50–66. https://doi.org/10.1016/j.brainres.2018.12.031.

39. Hayat, H., Regev, N., Matosevich, N., Sales, A., Paredes-Rodriguez, E., Krom, A.J., Bergman, L., Li, Y., Lavigne, M., Kremer, E.J., et al. (2020). Locus coeruleus norepinephrine activity mediates sensory-evoked awakenings from sleep. Sci. Adv. *6*, eaaz4232. https://doi.org/10.1126/sciadv.aaz4232.

40. Takeuchi, T., Duszkiewicz, A.J., Sonneborn, A., Spooner, P.A., Yamasaki, M., Watanabe, M., Smith, C.C., Fernández, G., Deisseroth, K., Greene, R. W., and Morris, R.G.M. (2016). Locus coeruleus and dopaminergic consolidation of everyday memory. Nature *537*, 357–362. https://doi.org/10.1038/nature19325.

41. Sciolino, N.R., Hsiang, M., Mazzone, C.M., Wilson, L.R., Plummer, N.W., Amin, J., Smith, K.G., McGee, C.A., Fry, S.A., Yang, C.X., et al. (2022). Natural locus coeruleus dynamics during feeding. Sci. Adv. *8*, eabn9134. https://doi.org/10.1126/sciadv.abn9134.

42. Aston-Jones, G., and Cohen, J.D. (2005). An integrative theory of locus coeruleus-norepinephrine function: adaptive gain and optimal performance. Annu. Rev. Neurosci. *28*, 403–450. https://doi.org/10.1146/annurev.neuro.28.061604.135709.

43. Stephenson, R., Liao, K.S., Hamrahi, H., and Horner, R.L. (2001). Circadian rhythms and sleep have additive effects on respiration in the rat. J. Physiol. *536*, 225–235. https://doi.org/10.1111/j.1469-7793.2001.00225.x.

44. Buchanan, G.F. (2013). Timing, sleep, and respiration in health and disease. Prog. Mol. Biol. Transl. Sci. *119*, 191–219. https://doi.org/10.1016/B978-0-12-396971-2.00008-7.

45. Aoki, S., Smith, J.B., Li, H., Yan, X., Igarashi, M., Coulon, P., Wickens, J.R., Ruigrok, T.J., and Jin, X. (2019). An open cortico-basal ganglia loop allows limbic control over motor output via the nigrothalamic pathway. Elife *8*, e49995. https://doi.org/10.7554/eLife.49995.

46. Alexander, G.E., DeLong, M.R., and Strick, P.L. (1986). Parallel organization of functionally segregated circuits linking basal ganglia and cortex. Annu. Rev. Neurosci. *9*, 357–381. https://doi.org/10.1146/annurev.ne.09.030186.002041.

47. Haber, S.N. (2003). The primate basal ganglia: parallel and integrative networks. J. Chem. Neuroanat. *26*, 317–330. https://doi.org/10.1016/j.jchemneu.2003.10.003.

48. Daviu, N., Bruchas, M.R., Moghaddam, B., Sandi, C., and Beyeler, A. (2019). Neurobiological links between stress and anxiety. Neurobiol. Stress *11*, 100191. https://doi.org/10.1016/j.ynstr.2019.100191.

49. Yackle, K., Schwarz, L.A., Kam, K., Sorokin, J.M., Huguenard, J.R., Feldman, J.L., Luo, L., and Krasnow, M.A. (2017). Breathing control center neurons that promote arousal in mice. Science *355*, 1411–1415. https://doi.org/10.1126/science.aai7984.

50. Richter, D.W., and Smith, J.C. (2014). Respiratory rhythm generation in vivo. Physiology *29*, 58–71. https://doi.org/10.1152/physiol.00035.2013.

51. Caggiano, V., Leiras, R., Goñi-Erro, H., Masini, D., Bellardita, C., Bouvier, J., Caldeira, V., Fisone, G., and Kiehn, O. (2018). Midbrain circuits that set locomotor speed and gait selection. Nature *553*, 455–460. https://doi.org/10.1038/nature25448.

52. Herent, C., Diem, S., Usseglio, G., Fortin, G., and Bouvier, J. (2023). Upregulation of breathing rate during running exercise by central locomotor circuits in mice. Nat. Commun. *14*, 2939. https://doi.org/10.1038/s41467-023-38583-6.

53. Lima, J.C., Oliveira, L.M., Botelho, M.T., Moreira, T.S., and Takakura, A.C. (2018). The involvement of the pathway connecting the substantia nigra, the periaqueductal gray matter and the retrotrapezoid nucleus in breathing control in a rat model of Parkinson's disease. Exp. Neurol. *302*, 46–56. https://doi.org/10.1016/j.expneurol.2018.01.003.

54. Subramanian, H., Huang, Z.G., and Balnave, R. (2008). Responses of brainstem respiratory neurons to activation of midbrain periaqueductal gray in the rat. Adv. Exp. Med. Biol. *605*, 377–381. https://doi.org/10.1007/978-0-387-73693-8_66.

55. Saunders, A., Macosko, E.Z., Wysoker, A., Goldman, M., Krienen, F.M., de Rivera, H., Bien, E., Baum, M., Bortolin, L., Wang, S., et al. (2018). Molecular Diversity and Specializations among the Cells of the Adult Mouse Brain. Cell *174*, 1015–1030.e16. https://doi.org/10.1016/j.cell.2018.07.028.

56. Nattie, E., and Li, A. (2012). Central chemoreceptors: locations and functions. Compr. Physiol. *2*, 221–254. https://doi.org/10.1002/cphy.c100083.

57. Guyenet, P.G., Stornetta, R.L., Souza, G.M.P.R., Abbott, S.B.G., Shi, Y., and Bayliss, D.A. (2019). The Retrotrapezoid Nucleus: Central Chemoreceptor and Regulator of Breathing Automaticity. Trends Neurosci. *42*, 807–824. https://doi.org/10.1016/j.tins.2019.09.002.

58. Brust, R.D., Corcoran, A.E., Richerson, G.B., Nattie, E., and Dymecki, S.M. (2019). Functional and developmental identification of a molecular subtype of brain serotonergic neuron specialized to regulate breathing dynamics. Cell Rep. *9*, 2152–2165. https://doi.org/10.1016/j.celrep.2014.11.027.

59. Klapoetke, N.C., Murata, Y., Kim, S.S., Pulver, S.R., Birdsey-Benson, A., Cho, Y.K., Morimoto, T.K., Chuong, A.S., Carpenter, E.J., Tian, Z., et al. (2014). Independent optical excitation of distinct neural populations. Nat. Methods *11*, 338–346. https://doi.org/10.1038/nmeth.2836.

60. Quattrochi, J.J., Mamelak, A.N., Madison, R.D., Macklis, J.D., and Hobson, J.A. (1989). Mapping neuronal inputs to REM sleep induction sites with carbachol-fluorescent microspheres. Science *245*, 984–986. https://doi.org/10.1126/science.2475910.

61. Riddle, D.R., Lo, D.C., and Katz, L.C. (1995). NT-4-mediated rescue of lateral geniculate neurons from effects of monocular deprivation. Nature *378*, 189–191. https://doi.org/10.1038/378189a0.

62. Wiltschko, A.B., Gage, G.J., and Berke, J.D. (2008). Wavelet filtering before spike detection preserves waveform shape and enhances single-unit discrimination. J. Neurosci. Methods *173*, 34–40. https://doi.org/10.1016/j.jneumeth.2008.05.016.

STAR★METHODS

KEY RESOURCES TABLE

REAGENT or RESOURCE	SOURCE	IDENTIFIER
Antibodies		
GFP antibody, Alexa FluorTM 647	Thermo Fisher Scientific	Cat# A-31852; RRID:AB_162553
GFP antibody, Alexa FluorTM 555	Thermo Fisher Scientific	Cat# A-31851; RRID:AB_2536188
TH antibody-rabbit	Millipore	Cat# AB152; RRID:AB_390204
Parvalbumin antibody-sheep	Thermo Fisher Scientific	Cat# PA5-47693; RRID:AB_2609239
Secondary Antibody, Alexa Fluor 350 (Donkey anti Rabbit IgG)	Thermo Fisher Scientific	Cat# A10039, RRID:AB_2534015
Secondary Antibody, Alexa Fluor 647 (Donkey anti Rabbit IgG)	Thermo Fisher Scientific	Cat# A-31573, RRID:AB_2536183
Secondary Antibody, Alexa Fluor 350 (Donkey anti sheep IgG)	Thermo Fisher Scientific	Cat# A-21097, RRID:AB_2535751
Bacterial and virus strains		
rAAV5-EF1α-DIO-hChR2(H134R)-eYFP	Addgene	Addgene plasmid # 20298-AAV5; RRID:Addgene_20298
rAAV2-EF1α-DIO-hChR2(H134R)-eYFP	UNC Vector Core	N/A
rAAV5-Syn-FLEX-ChrimsonR-tdTomato	Klapoetke et al.[59]	Addgene plasmid # 62723-AAV5; RRID:Addgene_62723
rAAV2-EF1α-DIO-eYFP	Addgene	Addgene plasmid # 27056-AAV2; RRID:Addgene_27056
Experimental models: Organisms/strains		
Gad2tm2(cre)Zjh/J mice	Jackson Laboratory	RRID:IMSR_JAX:010802
B6.129P2-Pvalbtm1(cre)Arbr/J mice	Jackson Laboratory	RRID:IMSR_JAX:017320
stock Tg(Dbh-Cre)KH212Gsat/Mmucd mice	MMRRC	RRID:MMRRC_032081-UCD
Software and algorithms		
Offline Sorter	Plexon Inc.	RRID:SCR_000012; https://plexon.com/products/offline-sorter/
MATLAB	Mathworks	RRID:SCR_001622; https://www.mathworks.com/
Intan RHD2000 recording system	Intan technologies	RRID:SCR_019278; https://intantech.com/downloads.html?tabSelect=Software
Other		
DAPI Fluoromount-G	SouthernBiotech	Cat# 0100-20
Red Retrobeads™	Lumafluor Inc. Quattrochi et al.[60] Riddle et al.[61]	N/A
Single-shank 16-channel electrodes	NeuroNexus	Cat# A1X16-10mm-100-177-A16
4-shank 32-channel electrodes	NeuroNexus	Cat# A4X8-5mm-100-200-177
Tungsten electrode	A-M Systems	Cat# 795500
DiI (DiIC$_{18}$(3)) electrode marker	Thermo Fisher Scientific	Cat # D3911
DiR (DiOC$_{18}$(7)) electrode marker	Thermo Fisher Scientific	Cat # D12731

EXPERIMENTAL MODEL AND SUBJECT DETAILS

Subjects

All animal procedures were performed in accordance with relevant institutional guidelines and national regulations governing animal research. The experimental protocols were approved by the Stanford University Administrative Panel on Animal Care (APLAC) and conducted in compliance with the National Institutes of Health Guide for the Care and Use of Laboratory Animals. Every effort was made to minimize animal suffering and to reduce the number of animals used. Experiments were performed with 3-12 month-old

male and female mice. Strains used were Gad2-Cre (Jackson Laboratory stock 010802, Gad2tm2(cre)Zjh/J, 12 male, 2 female), Pvalb-Cre (Jackson Laboratory stock 017320, B6.129P2-Pvalbtm1(cre)Arbr/J, 8 male, 3 female), and Dbh-Cre (MMRRC_032081-UCD, stock Tg(Dbh-Cre)KH212Gsat/Mmucd, 8 male, 2 female). The mice were housed in a 12-hour light-dark cycle with food and water provided *ad libitum*. All experimental groups had similar male-to-female ratios to control for potential sex differences, however sex was not analyzed as a variable due to sample size constraints.

METHOD DETAILS

Virus injections and stereotaxic surgery

Virus injection was performed using a stereotaxic frame with a heating pad, under stable anesthesia using 1.2% isoflurane with 100% oxygen. For the Gad2-Cre and Pvalb-Cre mice, rAAV5-EF1α-DIO-hChR2(H134R)-eYFP (0.4μl, $4x10^{12}$ titer), or rAAV2-EF1α-DIO-hChR2(H134R)-eYFP (0.2μl, $4x10^{12}$ titer) was injected into the left SN (AP: -3.25mm, LR: 1.3mm, DV: 4.7mm from Bregma). For the Dbh-Cre mice, rAAV5-Syn-FLEX-ChrimsonR-tdTomato[59] (0.3μl, $2x10^{13}$ titer) was injected into the left LC (AP: -5.4mm, LR: 0.85mm, DV: 3.9mm from Bregma). Virus was injected slowly (50 nl/min) using a 34 gauge needle attached to a NanoFil syringe (World Precision Instruments, FL) controlled by a microsyringe pump (Micro 4, World Precision Instruments, FL). After the injection was completed, 5-10 min was allowed to elapse before the needle was withdrawn, to prevent backflow. Post-surgery, the scalp was sutured, and the animals were monitored closely. Carprofen (5 mg/kg) and Buprenorphine sustained release (0.5 mg/kg, s.c.) were administered to alleviate pain and discomfort. If any signs of pain in the mice were observed, including redness or swelling around the surgical site, decreased or increased spontaneous activity, increased aggressiveness when handled, twitching, trembling, tremor, reduced grooming, abnormal posture, dehydration, weight loss, or abnormal breathing, further analgesia was provided as needed.

Acute electrophysiology with optogenetics

Three weeks after virus injection, mice were anesthetized using isoflurane (3% during induction, 1.2% during surgery, and less than 1% during optogenetic stimulation and recording), with 75% medical air (0.6 liter/min) mixed with 25% oxygen (0.2 liter/min). On a stereotaxic frame, body temperature was maintained at 37°C with a temperature controller (TCAT-2, Physitemp, during surgery) or an isothermal pad (Deltaphase, during optogenetic stimulation and recording). Craniotomies for SN and LC were made for electrode insertion, and the reference screw was inserted into the skull over the right cerebellum. For electrophysiological recordings, NeuroNexus single-shank 16-channel or 4-shank 32-channel electrodes were used, with 100 μm spacing between recording sites and 200 μm spacing between shanks. To construct optrodes, an optic fiber with 105-μm diameter was attached to the NeuroNexus probe, with the optic fiber tip positioned 1 mm above the electrode tip. SN electrode tips were targeted to the following coordinates: AP: -3.25 mm; LR: 1.3 mm for 16-channel electrodes, 1.0-1.6 mm for 32-channel electrodes; DV: 5mm from Bregma. LC electrode tips were targeted to the following coordinates: AP: -5.4 mm; LR: 0.85 mm for 16-channel electrodes, 0.5-1.1 mm for 32 channel electrodes; DV: 4mm from Bregma. To mark the electrode locations for histology, the electrodes were dipped in DiI ($DiIC_{18}(3)$) or DiR ($DiOC_{18}(7)$) stain solution immediately before insertion. Diaphragm EMG was recorded using a tungsten electrode with 0.002'' bare size and 1 mm uninsulated bended tip. The electrode was inserted through the lower intercostal space, proximal to the diaphragm, using a 28-gauge needle. Electrophysiology data from LC, SN, and diaphragm muscles were recorded simultaneously using an Intan RHD2000 recording system (Intan Technologies, wide-band of 0.79-7600 Hz, sampling rate of 20000/s).

Laser stimulation of SN in Gad2-Cre or Pvalb-Cre mice

The optic fiber on the optrode was connected to a 473 nm (blue light) laser (Laserglow Technologies). The laser power was adjusted so that the fiber tip would deliver 1.5 mW. Each mouse underwent 3-5 sessions of laser stimulation with simultaneous electrophysiology recordings of the SN, LC and diaphragm muscle. For each session, baseline recording was performed for 2-5 minutes, followed by 7 minutes of laser on – laser off cycles. For each cycle, the laser was turned on for 20 s (10Hz with 25ms laser pulse), then turned off for 40 s (number of cycles = 7). For some sessions, after the 7 cycles of laser stimulation, either dexmedetomidine or 7% CO_2 was delivered to the mice, and the measurements were repeated. When 7% CO_2 was used, the CO_2 was mixed into the gas supply and adjusted to 7% using an auxiliary air hose connected to a capnograph monitor (SurgiVet, V9004). After the CO_2 was turned on, 2.5 minutes were allowed to elapse so that the respiration pattern could stabilize. Then, 7 laser on – laser off cycles were repeated as above (Figure 4A). The dexmedetomidine experiment was done only as the last session, just before the animal was perfused. After injection of dexmedetomidine at a dose of 0.5mg/kg (s.c.), 2.5 minutes were allowed to elapse, followed by 7 laser on – laser off cycles as above (Figure 3A). Some of the Pvalb-Cre mice did not go through the laser stimulation session after dexmedetomidine injection (3 out of 11 mice).

Laser stimulation of LC in Dbh-Cre mice

The optic fiber on the optrode was connected to a 638 nm (red light) laser (Doric Lenses Inc). The laser power was adjusted so that the fiber tip would deliver 2 mW. Each mouse underwent 3-5 sessions of laser stimulation with electrophysiology recordings of LC and diaphragm muscle. For each session, baseline recording was performed for 2-5 minutes, followed by 7 minutes of laser on – laser off cycles (same parameters as SN stimulation).

Retrograde tracing studies

Red retrobeads™ IX (Lumafluor Inc.[60,61]) and AAV2-EF1α-DIO-eYFP (0.5ul, 3x1012 titer) was injected into two male Gad2-Cre mice for retrograde tract tracing. For labelling Gad2-expressing neurons in the Gad2-Cre mice, DIO-eYFP virus was injected into SN (AP: -3.25mm, LR: 1.3mm, DV: 4.7mm from Bregma). On the same day, retrobeads tracer was injected into LC (AP: -5.4mm, LR: 0.85mm, DV: 3.9mm from Bregma), followed by a three-week waiting period to allow full expression of the virus and tracer. The surgery procedure and post-surgery care followed the same protocol described in the surgery section.

Histology and immunofluorescence

Following electrophysiology recordings or retrograde tracing studies, mice were further deeply anesthetized and transcardially perfused with PBS followed by 4% paraformaldehyde (PFA). Brains were post-fixed in 4% PFA at 4°C for 12-24 hours, then sectioned into 50-μm coronal slices using either a cryostat microtome (Microm HM550, Thermo Fisher Scientific) or vibratome (Leica VT1000S). For viral expression verification and electrode placement, half of the brain sections were mounted with DAPI-containing medium (0100-20, SouthernBiotech) to visualize electrode tracks (DiI or DiR). The remaining sections underwent immunohistochemistry using various antibodies depending on the experiment.

For SN sections, eYFP antibody conjugated with Alexa Fluor™ 647 (A-31852, 1:400) or Alexa Fluor™ 555 (A-31851, 1:400) with DAPI was used. Some sections were double-immunostained using Pvalb-antibody (PA5-47693, 1:400) with secondary antibody (A-21097, Alexa Fluor 350, 1:400) and eYFP antibody to verify colocalization.

For LC sections in Gad2 and Pvalb-Cre mice, tyrosine hydroxylase (TH) antibody (AB152, 1:400) followed by secondary antibody (A31573, Alexa Fluor 647, 1:400) with DAPI was used to identify the LC.

For LC sections in Dbh-Cre mice, sections were stained using TH antibody (AB152, Sigma-Aldrich, 1:400), followed by secondary antibody (A10039, Alexa Fluor 350, 1:400), to verify that virus expression patterns matched the TH-stained LC area.

For retrograde tracing studies, LC sections were immunolabeled with TH antibody (AB152, 1:200) followed by secondary antibody (AB-150077, Alexa Fluor 488, 1:500), and SN sections with eYFP antibody conjugated with Alexa Fluor™ 647 (A-31852, Invitrogen, 1:400).

Brain sections were imaged using a widefield fluorescence microscope (Zeiss AxioImager) or confocal microscope (Zeiss LSM980) at the Neuroscience Microscopy Service at Stanford University.

QUANTIFICATION AND STATISTICAL ANALYSIS

Breathing and heart rate analysis

Diaphragm EMG signals were processed with MATLAB software to extract breathing and heart rates (Figures 1C and S3). Raw EMG signals were first bandpass filtered (10-450 Hz). Heartbeat locations were identified using peak detection (MATLAB 'findpeaks' function), and a "heart signal" was constructed by zeroing any signal more than 5 ms from any heartbeat. This heart signal was subtracted from the original EMG, and the remaining signal was filtered (150-350 Hz bandpass). A 200-ms sliding window standard deviation calculation was applied to obtain a "breathing signal." Breath locations were identified using peak detection. Manual spot checks were performed to ensure that heartbeats and breaths were accurately identified from the EMG signal. If any correction was required, the parameters of the Matlab function 'findpeaks' were adjusted until accuracy was achieved. Breathing and heart rates were calculated using a 10-s sliding window average. The breathing rate and heart rate time series data were zero centered, and any linear trend in each session (460s session data, starting 40s before the first laser onset) was removed using the MATLAB function 'detrend'.

Electrophysiological data analysis

Electrode placement was verified using histology. Signals from off-target electrodes were excluded from analysis. For unit categorization consistency, electrophysiological data from multiple recording sessions in each mouse were concatenated prior to analysis to enable uniform application of detection thresholds and classification criteria across all experimental conditions. For spike detection, signals were re-referenced using a common average across channels and wavelet-filtered before thresholding.[62] Detected spikes were sorted using Offline Sorter (Plexon Inc.), and low-amplitude or multi-units were excluded. All subsequent analyses, including statistical analysis, were performed using MATLAB. Firing rates of SN and LC units were normalized (z-scored) and binned into 1-s windows for laser block comparisons. For most of laser block comparison analyses, linear trends were removed from firing rate time series using the MATLAB 'detrend' function, in the same manner as was done for the breathing rate and heart rate comparisons. However, baseline firing rate comparisons of LC units (Figures 2G and 2H) utilized z-scored firing rates without detrending to enable direct comparison of baseline firing rates. LC unit data were temporally smoothed using a 10-s sliding window average to match the respiratory and heart rate time coordinates and to account for the low firing rates of LC neurons.

Categorization of LC units was done using spike width, firing rate, and response to dexmedetomidine. Units were categorized as putative NA cells if the half-width of spike shape was larger than the 200μs, mean firing rate was lower than 10 Hz, and there was reduced firing rate after dexmedetomidine injection (40-70s after injection) compared to before dexmedetomidine injection (0-30s before injection) (please see Figure S6 for the result using different criteria). Units with short half-width of spike shape (<200μs)

and mean firing rates over 10 Hz were defined as putative GABAergic cells. Other cells are classified as non-categorized. A few units were recorded without dexmedetomidine injection in the PV mice, and these were categorized as putative GABA neurons or non-categorized cells.

Categorization of SN units was done using Opto-tagging results and firing responses to the laser stimulus. A unit was defined as Opto-tagged if it showed significant increase of firing rate within 10ms after laser onset compared to the 25ms before laser onset (two-sided two-sample t-test, $P<0.001$) and there was high similarity between spike shapes during and outside of laser stimulation (Pearson's correlation coefficient $r > .90$, $n = 24$). The cells showing increased firing rates during the laser (25ms) compared to the 25ms before laser onset (two-sided two-sample t- test, $P<0.05$), but not categorized as Opto-tagged, were categorized as 'Increased (not tagged)'. Similarly, the cells with decreased firing rates during laser stimulation (during 25ms with laser stimulation compared to 25ms before laser onset, two-sided two-sample t-test, $P<0.05$) were categorized as 'Decreased', and the rest were defined as 'No change'. Opto-tagging of NA cells from the Dbh-Cre mice was done using the same methods as for the SN.